



Fine Secondary α Phase-Induced Strengthening in a Ti-5.5Al-2Zr-1Mo-2.5V Alloy Pipe with a Widmanstätten Microstructure

Guicheng Wu, Chun Feng, Huiqun Liu, Yonggang Liu, and Danqing Yi

(Submitted September 17, 2019; in revised form February 24, 2020; published online March 11, 2020)

In this paper, the Widmanstätten microstructure in an extruded near- α titanium alloy (Ti-5.5Al-2Zr-1Mo-2.5V) pipe was changed effectively by solid solution treatment at 920 °C for 2 h. The treatment produced intermittent lamellar α and discontinuous α grain boundaries (α_{GB}), and aging at 450 °C for 2 h introduced a high density of nanosized secondary α (α_s). The microstructure consisted of the lamellar α , α_{GB} and transformed β demonstrated a good combination of yield strength 1064 MPa and elongation 10.5%. Severe plastic deformation occurred inside the lamellar α during the tensile process, resulting in high-density dislocation tangles and dislocation cells. Furthermore, the stretching imposed on the tensile sample before aging generated dislocations, which piled up near the α/β interface. Thus, a coordinated deformation between lamellar α and transformed β , and the resultant strain partition contributed to an improvement in the ductility. Moreover, dislocation motion was effectively obstructed near the α/β interfaces, which dramatically strengthened the alloy. A solid solution at a middle temperature in the $\alpha + \beta$ region and aging at a low temperature provided an effective way to improve the strength and ductility simultaneously in titanium alloys with Widmanstätten microstructure.

Keywords aging, near- α titanium alloy, secondary α phase, solid solution, strength and ductility

1. Introduction

Titanium and its alloys are candidate materials for the petroleum, gas and chemical industries because of their high specific strength, high thermal stability, good weldability and excellent corrosion resistance (Ref 1-4). Due to the increasing difficulties encountered in drilling processes and the rapid development in the modern petroleum industry, there are increased requirements for drilling tools and materials. Some conventional drilling tools fail to satisfy the drilling requirements, and a range of drilling tools are designed to fulfill the demand for specific and complex wells. Titanium alloy drill pipes are a type of newly developed product that obtains the unique combination of the high strength and durability of a steel, as well as good flexibility, lightweight and good corrosion resistance (Ref 5-7). Due to the development of horizontal directional wells, extended-reach wells, deep-water wells, ultradeep wells and other critical projects, an increased yield strength for titanium alloy drill pipes is required (Ref 6-8).

Guicheng Wu, Huiqun Liu, and Danqing Yi, School of Materials Science and Engineering, Central South University, Changsha 410083, People's Republic of China; and State Key Laboratory of Powder Metallurgy, Central South University, Changsha 410083, People's Republic of China; and **Chun Feng and Yonggang Liu**, Tubular Goods Research Institute of CNPC, Xi'an 710065, People's Republic of China; and CNPC Key Laboratory for Petroleum Tubular Goods Engineering, Xi'an 710065, People's Republic of China. Contact e-mails: fengchun003@cnpc.com.cn and liuhuiqun@csu.edu.cn.

The mechanical properties can be effectively and favorably controlled by alloying and the microstructure tailored by heat treatment (Ref 4, 9, 10).

Generally, there are four typical microstructures for titanium alloys: equiaxed, bimodal, basket weave and Widmanstätten. These microstructures are distinguished by the morphology and content of the α phase (Ref 11, 12). The α phase shows three typical morphologies, namely equiaxed, lamellar and very fine acicular secondary α (α_s), which play a specific role in the mechanical properties. The equiaxed α that forms after plastic deformation and subsequent recrystallization annealing contributes to a high ductility and high cycle fatigue resistance. The lamellar α obtained from slow cooling in the β phase region has very good fatigue crack propagation resistance, fracture toughness and creep strength. The α_s precipitated during aging exhibits a strengthening effect because of an increase in the α/β interface (Ref 4, 13-15).

The most popular titanium alloy used for drill pipes is the Ti-6Al-4V alloy, which not only possesses the same high strength as steel drill pipes but also has a lightweight and good corrosion resistance; nevertheless, an increased strength is required due to increasing harsh drilling processes. Near- α titanium alloys possess a higher strength than Ti-6Al-4V alloy with a relatively high ductility (Ref 16). When titanium alloy ingots are extruded into pipes, they are often not plastically deformed to a large degree, so the strengthening measure generally involves a subsequent heat treatment, such as solid solution and aging treatments. The typical microstructure of an extruded Ti-6Al-4V or near- α titanium alloy consists of large lamellar α colonies and a continuous grain boundary α phase (α_{GB}) that shows Widmanstätten microstructure features. Some investigations demonstrated that a combination of high strength and high ductility can be achieved by generating a bimodal microstructure composed of an equiaxed α and transformed β matrix (β_T matrix) (Ref 17-19), and a large plastic deformation

is essential prior to heat treatment to induce equiaxed α (Ref 20). A large plastic deformation deviates from the typical post-extrusion treatment of pipes, and thus, this is not a feasible route. For near- α titanium alloys, a fully lamellar microstructure can be obtained through β heat treatment. Wu (Ref 19) found that controlling the cooling rate from the β phase region can produce lamellar α with different thicknesses. Lütjering (Ref 21) found that a fully lamellar microstructure in an IMI834 titanium alloy had a very high fracture toughness but low ductility. Additionally, thick lamellae in fully lamellar microstructures improve the fracture toughness of Ti-6Al-4V alloys since the rough profile at the crack front in a microstructure incorporating coarse α colonies and thick discontinuous α_{GB} triggers a higher crack growth resistance than that in microstructures with a thin α_{GB} (Ref 22). The coarse lamellar structure has a similar role in the deformation behavior as the equiaxed structure. In titanium alloys produced with powder metallurgy methods, coarse lamellar structures have been traditionally adopted to improve the ductility, but these structures sacrifice the strength (Ref 23, 24). The morphology and size of the α_s are very sensitive to the aging temperature and time. The size of α_s increased with increasing aging temperature, which led to a decrease in strength and an increase in ductility (Ref 25). Dispersed fine α_s precipitates in the β matrix exhibited an increased tensile strength due to the enormous α/β interfaces that decreased the effective slip length of the dislocations (Ref 14, 26, 27). Mantri (Ref 28) reported a very high tensile strength (UTS 1200-1810 MPa) in beta titanium alloys but a low elongation of 4-6.5% using solid solution and duplex aging treatments. Jia (Ref 29) reported an ultrahigh strength (UTS 1421 MPa) Ti-6Al-4V alloy with a relatively low elongation to fracture of 7.2% and a high oxygen level of 0.52 wt.%; the alloy was produced by powder compact forging, a solid solution treatment and aging. Hence, solid solution and aging treatments are a possible way to achieve a balance between strength and ductility for near- α titanium alloy pipes.

The aim of this work is to obtain an improved combination of strength and ductility for a near- α titanium alloy pipe comprising Ti-5.5Al-2Zr-1Mo-2.5V through a solid solution treatment in the $\alpha + \beta$ phase region and aging at a decreased temperature. Prestretching with a small deformation degree

before aging was applied to increase the dislocation density. The microstructure evolution during heat treatment was investigated using scanning electron microscopy (SEM) and transmission electron microscopy (TEM), according to which the origin of the good combination between strength and ductility was determined and is explained in detail.

2. Materials and Methods

The as-received near- α titanium specimen was an extruded pipe with an outer diameter of 89 mm, inner diameter of 69 mm and wall thickness of 10 mm, as shown in Fig. 1. Its chemical composition (wt.%) was 5.57 Al, 1.8 Zr, 0.83 Mo, 2.5 V, 0.038 Fe and the balance Ti. The β -transus temperature was measured as 970 °C by the metallographic method similar to Ref. 30; the value estimated by equation (Ref 31, 32) is 949 °C while not including the oxygen and other impurities. The value was 972 °C acquired by differential scanning calorimetry (DSC). Based on our experiments results, calculation and other research institutes, the $\alpha + \beta \rightarrow \beta$ transformation temperature (T_β) was 970 °C.

Considering the β -transus temperature and the influence of the holding temperature on the volume fraction and size of the lamellar α , a two-stage heat treatment including a solid solution treatment (ST) and aging stage (STA) was selected to tailor the microstructure. As shown in Fig. 2, a ST at 950, 930 and 920 °C was selected to control the content and size of the lamellar α phase through transformation of the α phase into the β phase. To reach the equilibrium of the α and β phases, a 2-h holding time was chosen. Water quenching after the solid solution treatment was done to avoid the precipitation of lamellar α and α_s . To generate additional nucleation sites for α_s precipitation, a prestretch of 2.5% was employed before the aging treatment. For the STA, the specimens were isothermally held at 450 °C to precipitate α_s . The heat treatment processing routes and the corresponding samples are illustrated in Fig. 2 and Table 1, respectively.

Cylindrical samples were machined from the pipe with 5 mm gage diameters and 25 mm gage lengths for heat treatment (Fig. 1b) (Ref 11). Prestretching before aging was

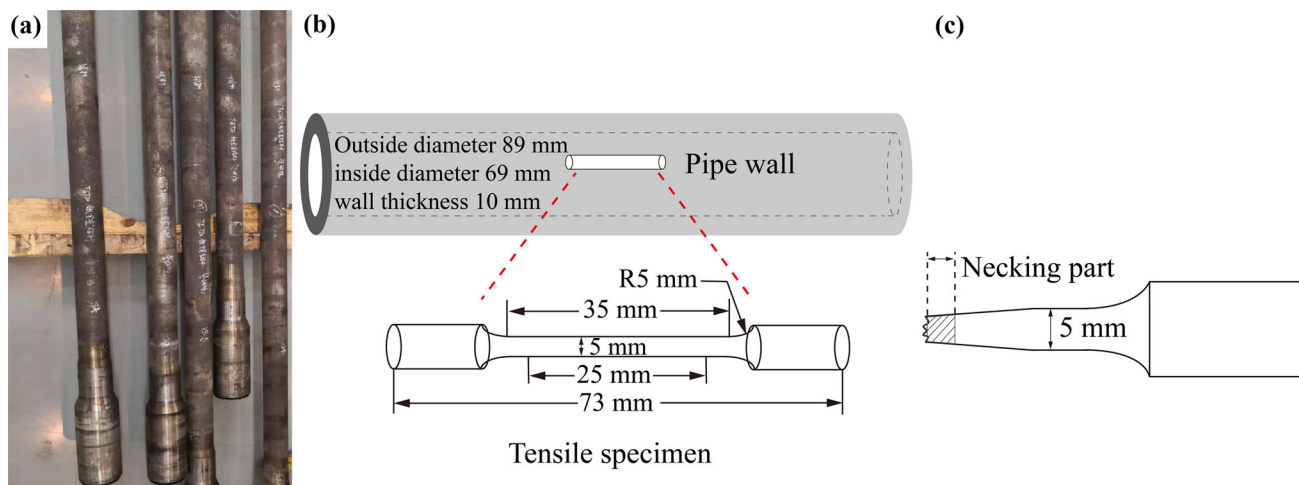


Fig. 1 Schematic of the specimen: (a) extruded pipe, (b) illustration of tensile specimen machined from pipe and (c) illustration of TEM foils machined from the part that experienced necking along the stretching direction

performed at room temperature using a strain rate of 2.5×10^{-4} with an extensometer on an MTS Landmark system. The yield strength (YS), ultimate tensile strength (UTS) and elongation (EL) were also determined on the MTS Landmark system at a strain rate of 6.67×10^{-4} .

The samples for metallographic analysis with optical microscopy (OM) and SEM examination were chemically etched in a solution of 10% HF + 10% HNO₃ + 80% H₂O for 5 s after grinding and polishing. The volume fraction of the lamellar α phase was quantified by Image-Pro Plus software. TEM (Tecnai G2 F20 TEM system operating at 200 kV) was also employed to observe the microstructures. The thin foils for TEM observation were machined from the necked part along the stretching direction (Fig. 1c) and thinned to 60 μ m in thickness. A twin-jet electropolisher was adopted to prepare the TEM foils with a chemical solution of 6% perchloric acid and 34% *n*-butyl alcohol and 60% methanol at -30 °C and 30 V.

3. Results

3.1 The Extruded Microstructure

Figure 3 shows the as-extruded microstructure of the Ti-5.5Al-2Zr-1Mo-2.5V alloy pipe. As shown in Fig. 3(a) and (b), the microstructure contains large lamellar α colonies and continuous α_{GB} phases. The primary lamellar α directly transformed during slow cooling from the β phase region or $\alpha + \beta$ phase region. Obasi (Ref 33) reported that 12 possible α orientations transformed from a single β grain following the Burgers orientation relationship $\{0002\}_\alpha // \{110\}_\beta$ and $\langle 1120 \rangle_\alpha // \langle 111 \rangle_\beta$, so α colonies with diverse orientations appeared. Figure 3(c) and (d) shows the TEM microstructure

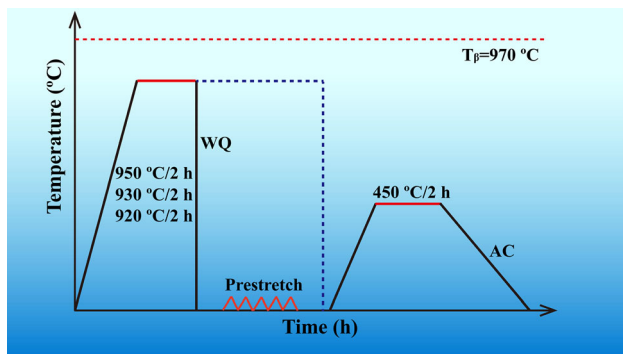


Fig. 2 The processing routes performed on the Ti-5.5Al-2Zr-1Mo-2.5V alloy

details of the lamellar α and residual β phase, which confirms that no α_s existed in the extruded alloy. Moreover, dislocations can be observed inside the coarse lamellar α , and dislocations slipped inside the coarse lamellar α grain interior, possibly producing a relatively good plastic deformation ability.

3.2 Evolution of the α Phase During the Solid Solution and Aging Treatments

Figure 4 displays the microstructure of the alloy sample after solid solution treatment at 920 °C for 2 h and water quenching that contained intermittent lamellar α and acicular α' martensite. As shown in Fig. 4(a) and (b), large lamellar α colonies dissolved and changed to the intermittent lamellar α during the high-temperature soaking stage, which was governed by the transformation of the $\alpha \rightarrow \beta$ phase to reach phase equilibrium. During the heating and holding stages, the tip of the lamellar α and thin lamella originated from the decomposition of the branched lamellar α transformed into the β phase with the diffusion of the alloying elements (Ref 34, 35). Additionally, as the temperature increased, the activated dislocations gradually developed into planar arrays and sub-grain boundaries to decrease the total energy, and some sub-grain boundaries dissolved due to the transformation of the $\alpha \rightarrow \beta$ phase as the solution time was prolonged, resulting in the splitting of the lamellar α (Ref 36, 37). The initiation of lamellar splitting occurred at the junction of the sub-grain boundaries, which caused grooves in the lamellar α , as shown by the yellow arrows in Fig. 4(a) and (b). Then, the initial lamellar α broke, and the α colonies transformed into intermittent lamellar α . The morphology of the lamellar α was preserved at high temperatures, mainly due to the lack of sufficient time for the lamellar α to grow and coarsen. However, the β phase transformed to α' martensitic after water quenching.

Figure 5 and 6 shows typical microstructures of the sample after solid solution treatment at 920 °C for 2 h and aging at 450 °C for 2 h (ST920A450) and also after solid solution treatment at 920 °C for 2 h, prestretching 2.5% and aging at 450 °C for 2 h (ST930S2.5A450). As shown in Fig. 5(a) and (b), some of the intermittent lamellar α was approximately parallel, indicating that these lamellar α exhibited the same orientation and belonged to the same initial α colony. Moreover, after holding at 920 °C for 2 h, the original continuous α_{GB} formed a zigzag shape and discontinuous morphology. The discontinuous α_{GB} also arose from the $\alpha \rightarrow \beta$ phase transformation. Through STA treatments, the original Widmanstätten structure changed to large lamellar α , discontinuous α_{GB} and α_s . For the ST920A450 sample, the mean width of the lamellar α was 1.3 μ m, the aspect ratio was 7.2:1, and the volume fraction of the α phase was approximately 27%. The volume fraction of the lamellar α decreased

Table 1 Samples heat-treated under different conditions

Sample	Solid solution treatment	Prestretching amount	Aging treatment
Extruded
ST920A450	920 °C/2 h/WQ	...	450 °C/2 h/AC
ST920S2.5A450	920 °C/2 h/WQ	2.5%	450 °C/2 h/AC
ST930A450	930 °C/2 h/WQ	...	450 °C/2 h/AC
ST930S2.5A450	930 °C/2 h/WQ	2.5%	450 °C/2 h/AC
ST950A450	950 °C/2 h/WQ	...	450 °C/2 h/AC

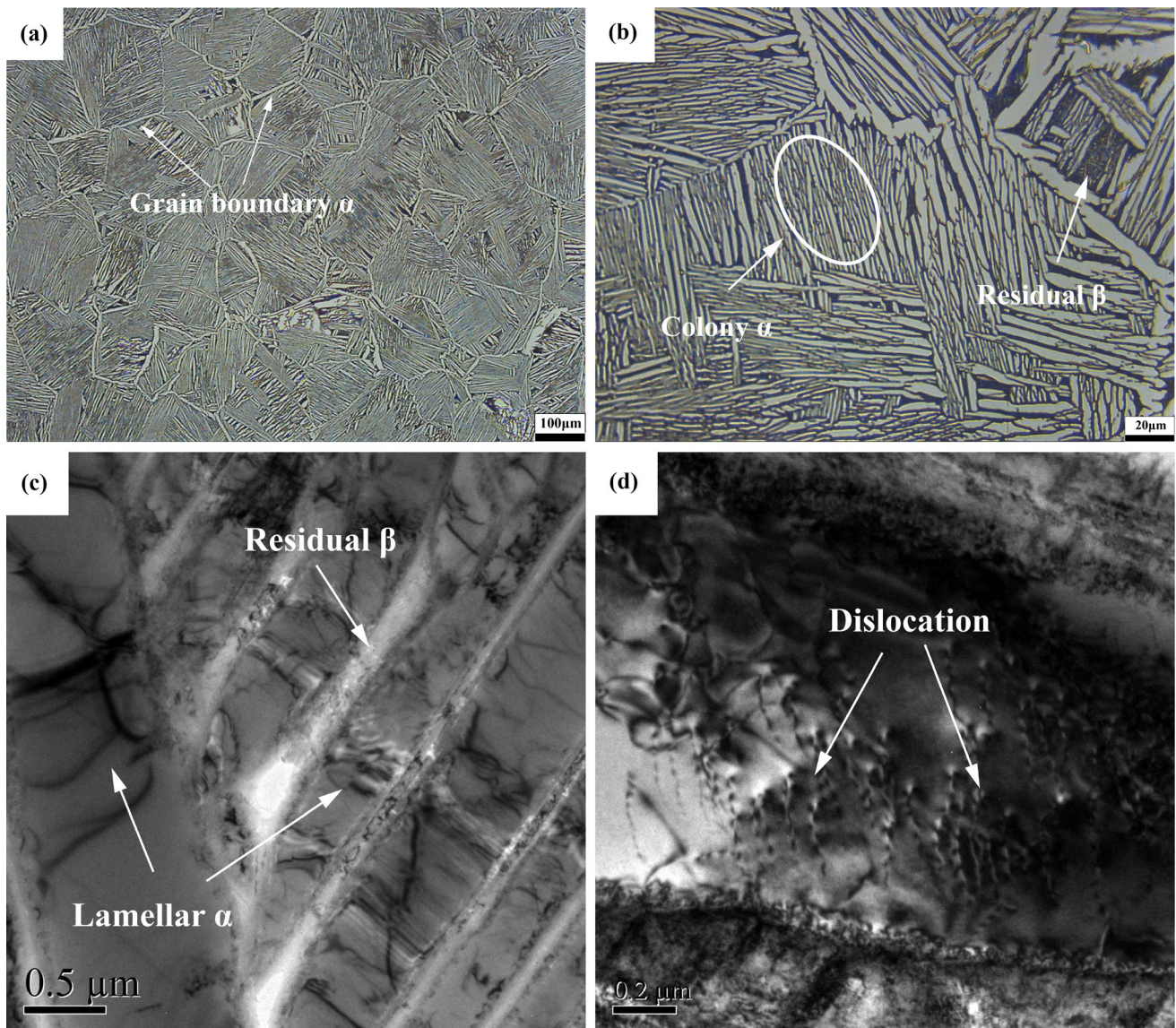


Fig. 3 As-extruded microstructure of the Ti-5.5Al-2Zr-1Mo-2.5V alloy pipe: (a) and (b) microstructure observed with OM, (c) and (d) morphology of the lamellar α and dislocations observed with TEM

from 93% in the extruded sample to 27% in the ST920A450 sample after the solid solution and aging treatments. With an elevated solid solution temperature, the volume fraction of the lamellar α in the ST930A450 sample was reduced to 20%, whereas little change occurred in the ST920S2.5A450 and ST930S2.5A450 samples, as displayed in Table 2. The higher the solid solution temperature was, the lower the volume fraction of the lamellar α .

After the solid solution treatment and water quenching, the β matrix was filled with acicular α' martensite that decomposed into α_s during the subsequent aging treatment; however, they could not be visibly distinguished from the SEM image mainly because of their small size relative to the primary α grains and low contrast with the matrix. However, through the TEM image shown in Fig. 5(c), it can be seen that a large amount of α_s was dispersed in the matrix. The secondary α phases had a long strip-like shape. Some of them were black and some were white, from the different colors arose from the different orientation relationships. After measuring more than 200 α_s phases, as shown in Fig. 5(e), the width of α_s was conformed to

be a normal distribution, and the mean value was 140 nm; this result implied that there were many nucleation sites for α_s precipitates during the aging treatment.

Figure 6 displays the microstructure of the ST930S2.5A450 sample, which consisted of lamellar α , discontinuous α_{GB} and α_s . Compared to the microstructure of the ST920A450 sample, the lamellar α showed a scattered distribution, the volume fraction was lower, and α_{GB} became more discontinuous. After the STA treatment, the width and aspect ratio of the lamellar α slightly decreased to 1.22 μm and 6.7:1, respectively, while the volume fraction of the α phase dropped by 20% due to the elevated solid solution temperature. A fine and uniform needle-like α_s precipitate is observed in Fig. 5(c), the mean width dropped by 51% to 68 nm, and the corresponding mean values of the ST920S2.5A450 and ST930A450 samples were 78 nm and 132 nm, respectively, as shown in Fig. 7(b) and (d), respectively. The average value of the α_s precipitate in the ST930A450 sample was marginally lower than that in the ST920A450 sample, whereas it was reduced markedly after the 2.5% prestretching process for the ST930S2.5A450 sample.

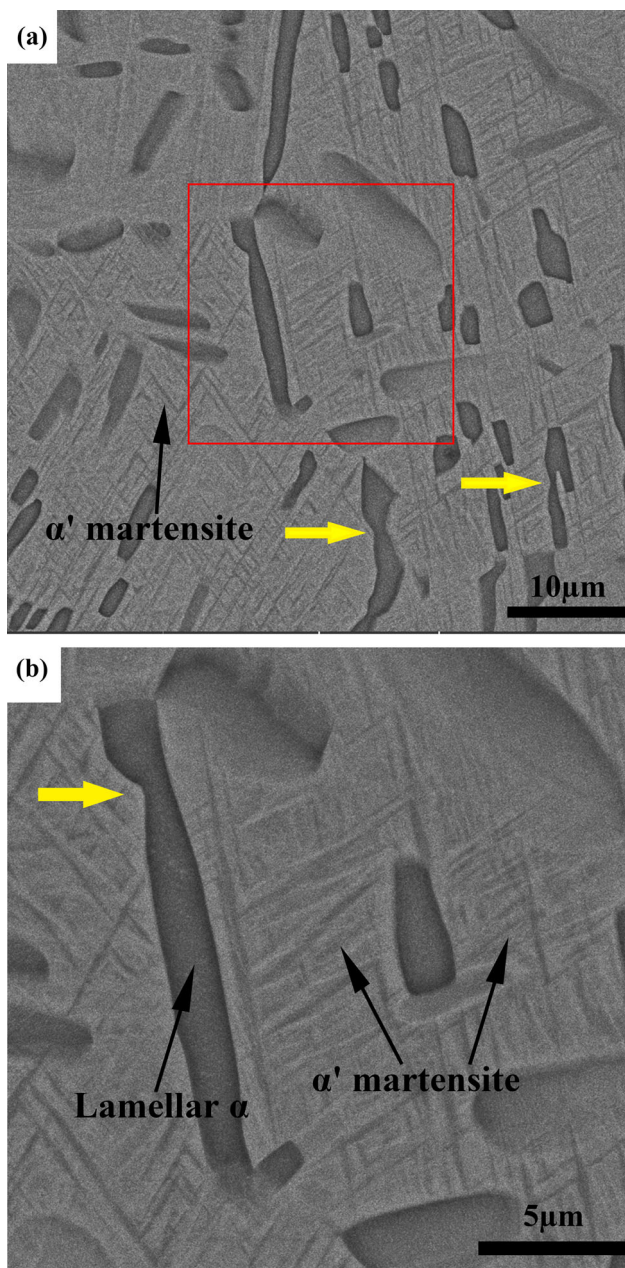


Fig. 4 Microstructure of the Ti-5.5Al-2Zr-1Mo-2.5V alloy after solid solution treatment at 920 °C for 2 h and water quenching: (a) SEM-BSE image showing the intermittent lamellar α and acicular α' martensite and (b) enlarged image of the red rectangle in (a) (Color figure online)

This result indicated that the prestretching was effective and generated a substantial number of defects that induced fine and uniform α_s precipitates during aging treatment. The more nucleation sites there are, the more α_s phase there is, and the smaller the size is. In contrast, there was a much smaller change between the ST920A450 and ST930A450 samples. Moreover, as shown in Fig. 7(f), the average width of the α_s precipitate of the ST950A450 sample was 177 nm, which is in good agreement with the strength decrease compared to that of the other samples. The solution treatment at the top of the $\alpha + \beta$ region or β region brought about a stable transformed β matrix and provided a high driving force for the subsequent decom-

position. In that case, the α_s precipitate was easier to nucleate and grow and resulted in an increased size (Ref 38).

3.3 Tensile Properties

The room temperature tensile curves of the extruded and heat-treated samples from the pipe specimens are presented in Fig. 8(a). The serration characteristics are visible in the stress-strain curves of the ST930S2.5A450 sample, ST920S2.5A450 sample, ST930A450 sample and ST920A450 sample, which were mainly derived from the different sizes of the α_s precipitates, prestretching history and shearing of the α_s precipitates. First, as mentioned in Sect. 3.2, different samples had different widths of the α_s precipitates. Dynamic strain aging (DSA) took place preferentially on the grain boundaries where local obstacles to dislocation motion formed. Moreover, in the coarse-grained samples, such as the ST920A450 sample, the dislocation density was low, and thus, the average dislocation velocity was higher in these samples than in the fine-grained samples at the same strain; thus, the serration characteristics occurred at elevated strains. Second, the dislocation density induced by prestretching exhibited a tendency to form a typical tangle structure, which helped to form the Portevin–Le-Chatelier (PLC) band and cause the serrated flow. Third, the α_s precipitates were sheared by the substantial pileup of dislocations with an increase in the applied stress, and then, a subsequent stress relaxation occurred after a definite duration. The repetition of this sequence led to successive stress drops and then to visible serrations (Ref 39).

The YS, UTS and elongation of the extruded sample with a lamellar α microstructure were 820, 950 MPa and 12%, respectively. The ST930S2.5A450 sample with a lamellar α and needle-like α_s microstructure exhibited an elevated YS that increased 56% to 1279 MPa; the increase was mainly induced by the large α_s/β interfaces. However, with increasing strength, the ductility decreased to 6.6%. The ST920A450 sample with a lamellar α , discontinuous α_{GB} and α_s microstructure achieved a good combination of strength (YS of 1064 MPa and UTS of 1256 MPa) and elongation of 10.5%; the YS was 242 MPa higher than that of the extruded sample, and the ST920A450 sample experienced a small decrease in the ductility. These results confirmed that the high strength mainly originated from dislocations that were hindered by the α_s/β interface; this finding is presented and discussed in the TEM images in an upcoming section. The decreased volume fraction of the lamellar α and fine dispersed α_s contributed an increased strength and good ductility. As shown in Fig. 8(b), in light of the requirement of ASTM B861 grade 5 for Ti-6Al-4V alloy drill pipe (YS of 828 MPa, UTS of 895 MPa and EL of 10%) (Ref 40), there is a great improvement in the strength in this work.

4. Discussion

4.1 High Ductility of the Extruded Sample and Ultrahigh Strength of the Aged Sample

The resultant plastic deformation during the tensile process generated parallel dislocation lines inside the coarse lamellar α , as indicated by the arrow in Fig. 9(a). With an additional applied strain, the dislocations became tangled through their interaction and rearrangement and gradually formed dislocation

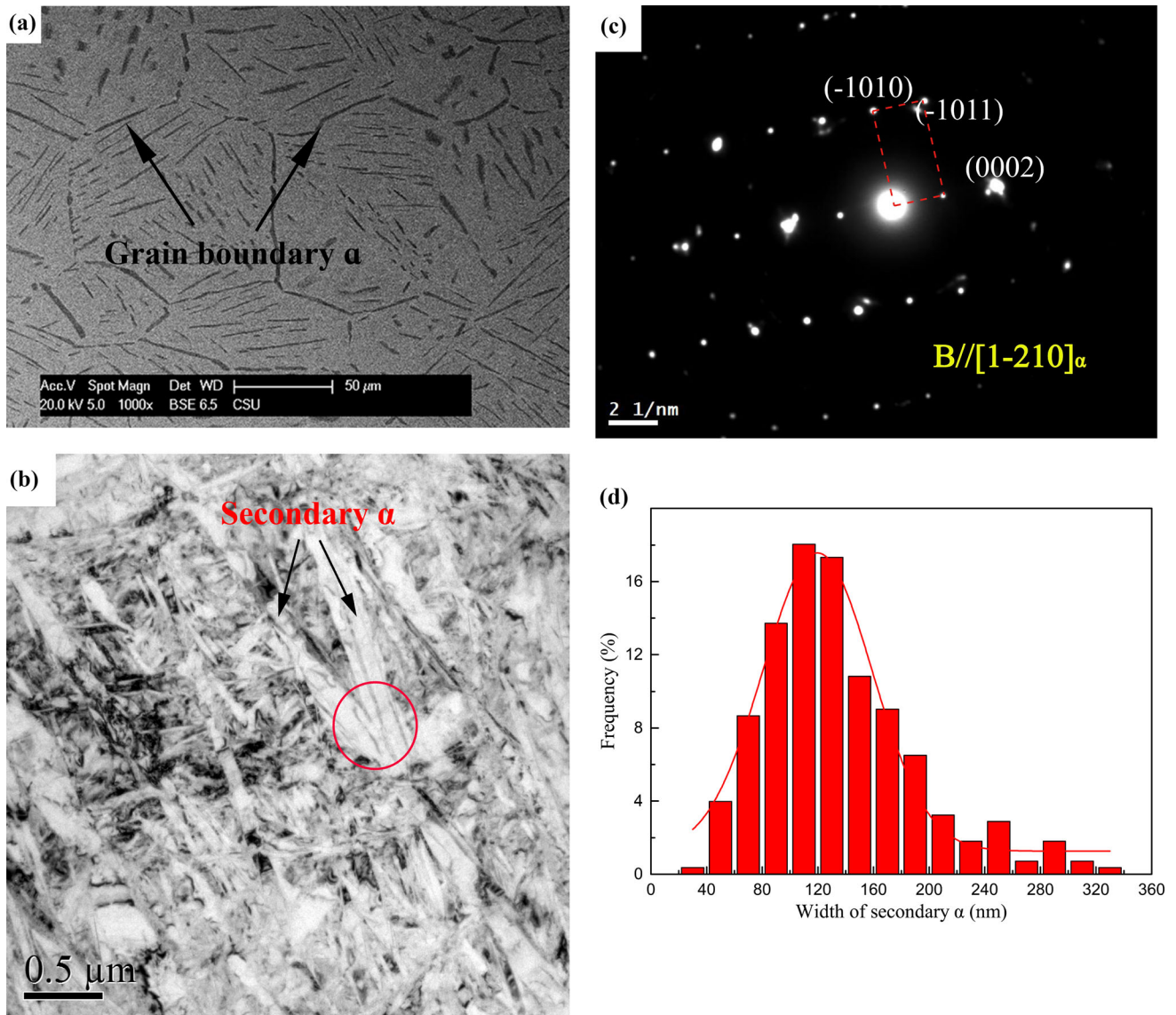


Fig. 5 Microstructure of the ST920A450 sample: (a) SEM image showing primary β grains, lamellar α and discontinuous α_{GB} ; (b) TEM image of the α_s ; (c) SAD pattern along the $[1\bar{2}10]_{\alpha}$ direction taken from the area within the red circle in (b); and (d) width distribution histogram for the α_s (Color figure online)

cells and walls, as shown in Fig. 9(b), which was observed after tensile testing of pure titanium (Ref 41, 42) and some titanium alloys (Ref 43, 44). Moreover, the dislocation density appeared decreased inside the dislocation cells, which implies that the dislocation walls and cell structure experienced an obstruction during dislocation motion. However, the existing mobile dislocations inside the dislocation walls and cells can still slip, and the slip length is the width of the dislocation walls and cell structure. The number of cell structures increased as the strain increased until fracture. Therefore, the successive occurrences of dislocation slip were beneficial to the ductility, and the formation of dislocation cells and wall structures resulted in an increase in the tensile strength.

Furthermore, a great deal of lamellar α coordinated the deformation, inhibiting the stress concentration in favorable grains, which possibly induced crack initiation. As presented in Fig. 3(a) and (b), the prior β interior incorporated a multitude

of α grains with different sizes. The accommodation of α grains also contributed to the good ductility.

The high strength (UTS 1328 MPa) of the ST930S2.5A450 sample mainly resulted from the nanosized dispersed α_s . The volume fraction of lamellar α decreased from 27 to 20% due to the higher temperature of the solid solution treatment at 930 $^{\circ}\text{C}$ than that of the ST920A450 sample; moreover, the width of the lamellar α decreased to 1.22 μm , which further constrained the dislocation motion inside lamellar α . Also, the 2.5% prestretching produced many additional defects, such as dislocations, which provided nucleation sites for the α_s precipitates (Ref 45, 46). With an increase in the number of nucleation sites, the α' martensite decomposed into fine and uniform α_s after the sample was aged at 450 $^{\circ}\text{C}$, as shown in Fig. 6(b) and (d). The width of the α_s decreased from 140 nm to 68 nm in the ST920S2.5A450 sample, resulting in an increase in the interface between the α and β phases, which played a similar role as the grain boundaries in constraining the dislocation

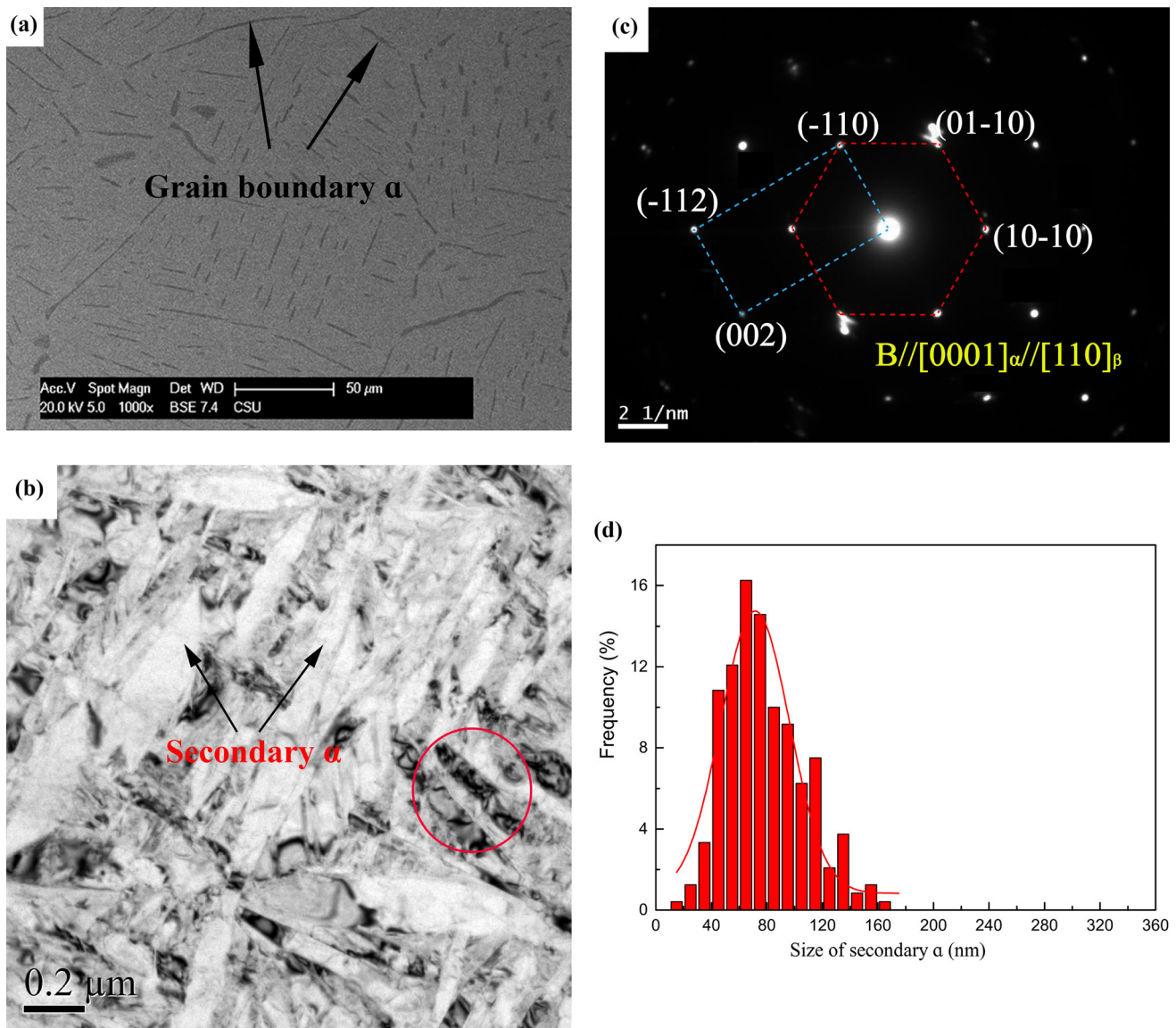


Fig. 6 Microstructure of the ST930S2.5A450 sample: (a) SEM image showing the primary β grains, lamellar α and discontinuous α_{GB} ; (b) TEM image of the α_s ; (c) SAD pattern along the $[0001]_{\alpha}$ direction taken from the area within the red circle in (b); and (d) width distribution histogram for the α_s (Color figure online)

Table 2 The volume fractions of lamellar α

Sample	Amount of lamellar α , %
Extruded	93
ST920A450	27
ST920S2.5A450	26.5
ST930A450	19
ST930S2.5A450	20
ST950A450	8

motion. Therefore, the high strength of the ST930S2.5A450 sample was obtained from the fine and uniform α_s precipitates (~ 68 nm), but the ductility decreased to 6.6%.

4.2 A Promising Combination of Strength and Ductility

A good combination of strength and ductility in the ST920A450 sample is displayed in Fig. 8. The enhanced UTS (1256 MPa) was achieved through the high-density and fine α_s . The UTS was improved by 300 MPa compared to that of the extruded sample. The microstructure of the ST920A450 sample contained lamellar α , nanosized α_s and discontinuous α_{GB} , as shown in Fig. 5.

It is well known that solid solution strengthening, grain boundary strengthening and precipitation strengthening are the main strengthening mechanisms in alloys. In most titanium alloys, α/β interface strengthening is the dominant mechanism (Ref 47, 48), and precipitation strengthening controlled by the Orowan mechanism is weak. Figure 8(a) shows 244 MPa improvement in the YS for the ST920A450 sample in comparison with that of the extruded sample. A reasonable explanation is that the strength increase was dominated by the α/β interface. The interface strengthening mechanism is similar

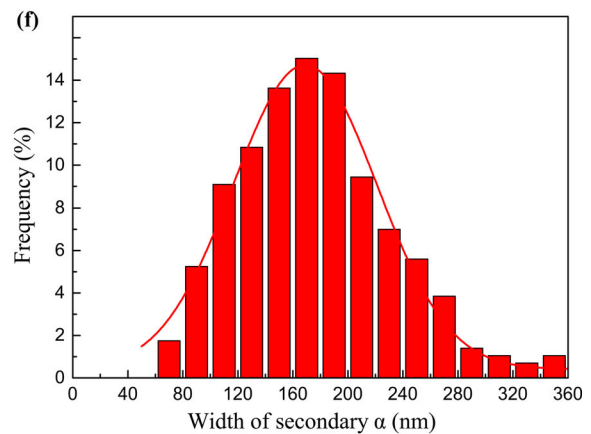
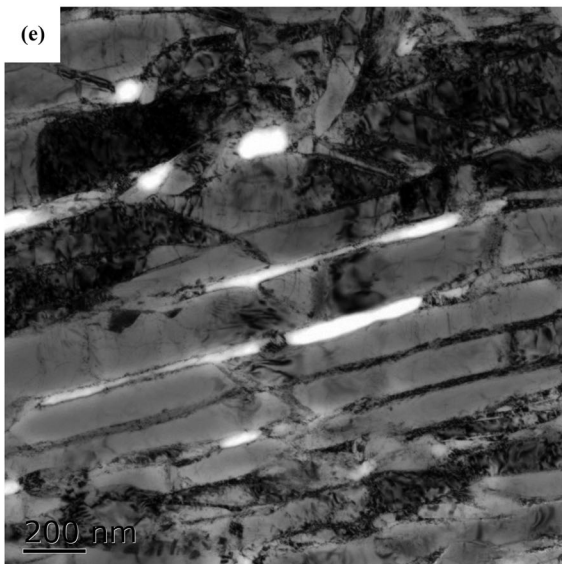
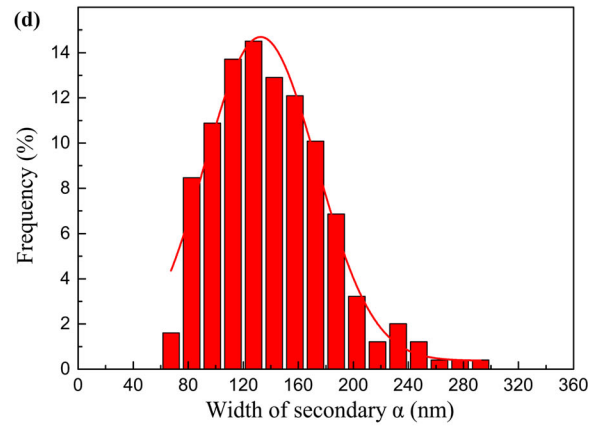
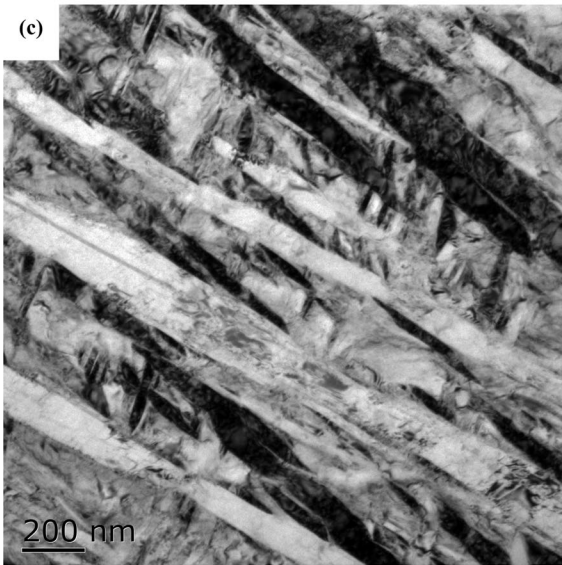
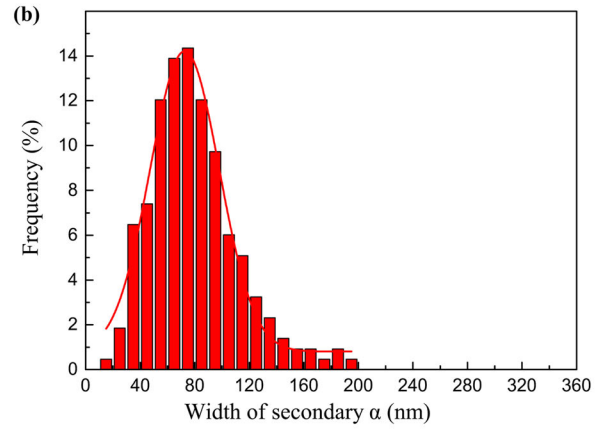
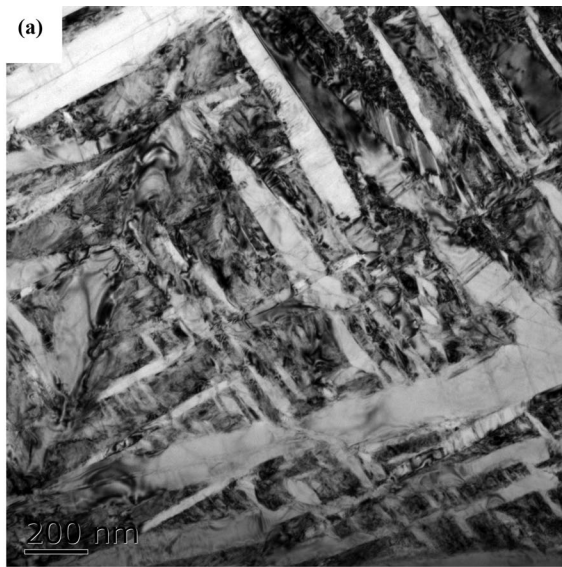
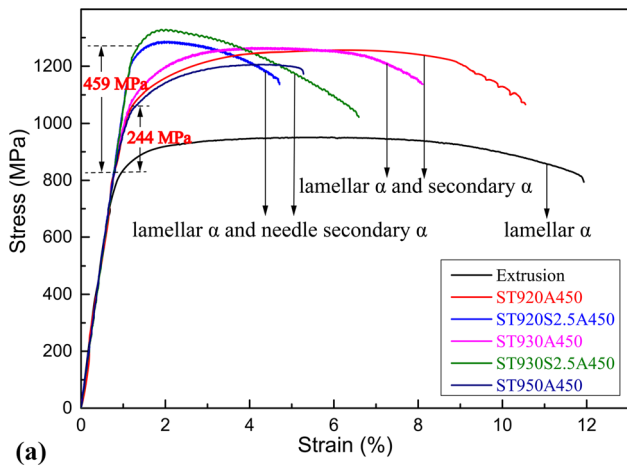
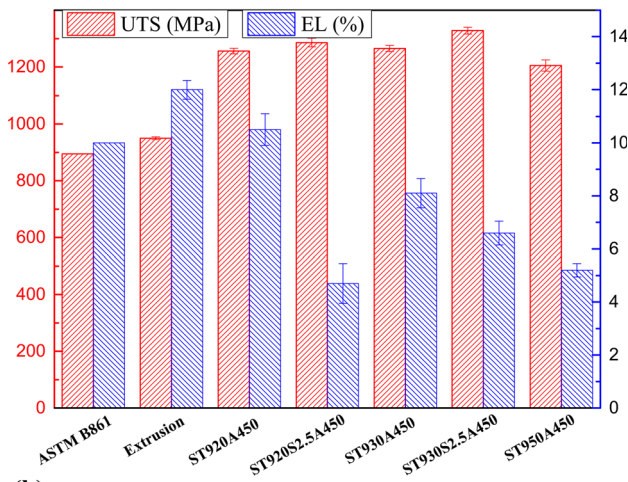


Fig. 7 Microstructure of samples: (a) TEM image of α_s in the ST920S2.5A450 sample; (b) width distribution histogram of the corresponding α_s in (a); (c) TEM image of α_s in the ST930A450 sample; (d) width distribution histogram of the corresponding α_s in (c); (e) TEM image of α_s in the ST950A450 sample; and (f) width distribution histogram of the corresponding α_s in (e)



(a)



(b)

Fig. 8 Tensile properties of the Ti-5.5Al-2Zr-1Mo-2.5V alloy: (a) engineering stress-strain curves of the extruded and heat treated samples and (b) UTS and EL of the samples compared with those in the ASTM B861 standard

to the fine grain effect, where the α/β interfaces played the same role as the grain boundaries, where dislocations piled up at the grain boundaries. The Hall-Petch relation $\sigma_y = \sigma_0 + kd^{-1/2}$ (Ref 49) was employed to estimate the strength, where σ is the yield strength of tested samples, σ_0 is the friction stress of a single crystal, and $kd^{-1/2}$ represents the grain boundary strengthening (k is the Hall-Petch slope and d is the average size of the lamellar microstructure) (Ref 50). The value of “ d ” dramatically decreased from the width of coarse lamellar α (5.4 μm for the extruded sample) to the mean width of α_s (0.14 μm for the ST920A450 sample, 0.078 μm for the ST920S2.5A450 sample, 0.132 μm for the ST930A450 sample, 0.068 μm for the ST930S2.5A450 sample and 0.177 μm for the ST950A450 sample), as shown in Fig. 10. The yield strength increased with decreasing α_s width, which demonstrated that the width of the α_s played a critical role in the strength improvement. Figure 10 displays the plot of measured YS (σ_y) versus $d^{-1/2}$; the relationship is approximately linear, which validates the Hall-Petch-type analysis. From this relationship, the σ_0 is found to be ~ 754 MPa and the Hall-Petch strengthening coefficient k could be estimated to be about 4140 MPa nm $^{1/2}$. This is in close agreement with the coeffi-

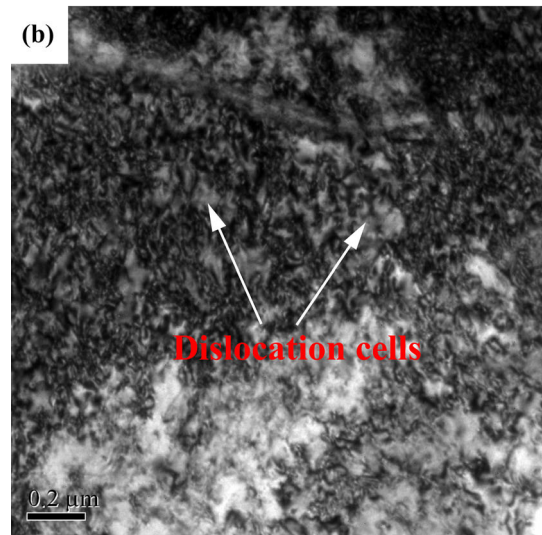
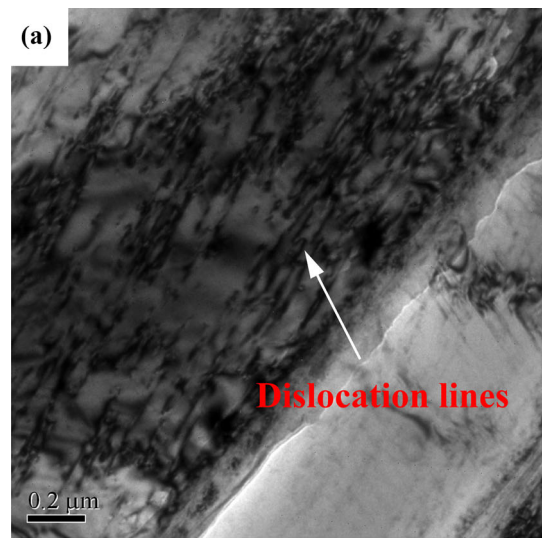


Fig. 9 Typical bright-field TEM images of the extruded microstructure after tensile testing at the part that experienced necking: (a) dislocation lines within the lamellar α phase and (b) highly tangled dislocations inside the lamellar α phase and near the grain boundaries

cient value of 4490 MPa nm $^{1/2}$ for Ti-6Al-4V alloy in Ref 43; another value of k can be found 16,316 MPa nm $^{1/2}$ for Ti-6Al-4V alloy in Ref 51, but it was subjected to multidirectional isothermal forging (MDIF). Other estimations of k can be estimated as 54,000 MPa nm $^{1/2}$ for Ti-35Nb-2Zr-0.5O alloy (Ref 52), 11,400 MPa nm $^{1/2}$ for pure Ti (Ref 53) and 2615 MPa nm $^{1/2}$ for β -21S alloy (Ref 28). In general, equiaxed and lamellar α is softer than a β -transformed structure, where a high density of nanosized α_s transformed from α' martensite and β , resulting in an increased number of α/β interfaces. As shown in Fig. 11(a), a high density of tangled dislocations piled up at the α/β interface with additional tensile deformation; thus, dislocation motion in the β -transformed structures was constrained into a large number of small regions. The effective slip length sharply dropped to the spacing of the nanosized precipitates (140 nm); generally, the yield strength increases with a decrease in the effective slip length (Ref 21), which in turn significantly strengthens the alloy.

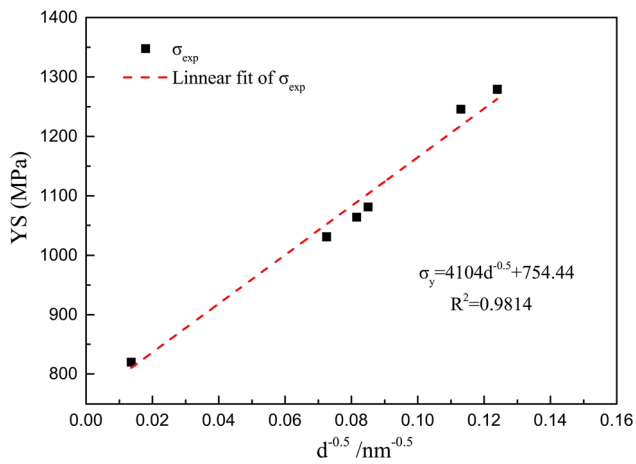


Fig. 10 The dependence of σ on $d^{-0.5}$ in the samples

Dislocation slip was believed to initiate from the soft lamellar α compared to the hard β -transformed structures. Figure 11(b) shows the characteristics of the dislocations inside the lamellar α after tensile deformation. The lamellar α interior consisted of a great number of tangled dislocations and dislocation cells, which demonstrated that severe plastic deformation occurred inside the lamellar α during tensile deformation, as discussed in Sect. 4.2. Furthermore, tilting the foil from the electron beam direction of $[1\bar{2}10]$ in Fig. 11(b) to $[0002]$ in Fig. 11(d), it can be observed that highly tangled dislocations were distributed throughout the lamellar α , which implied that the lamellar α exhibited a good plastic deformation capability during tensile deformation. Additionally, the wavy dislocation configuration indicated that frequent cross-gliding occurred (Ref 54, 55). To some extent, these highly tangled dislocations hindered further gliding, leading to a strength improvement. On the other hand, the original α_{GB} changed

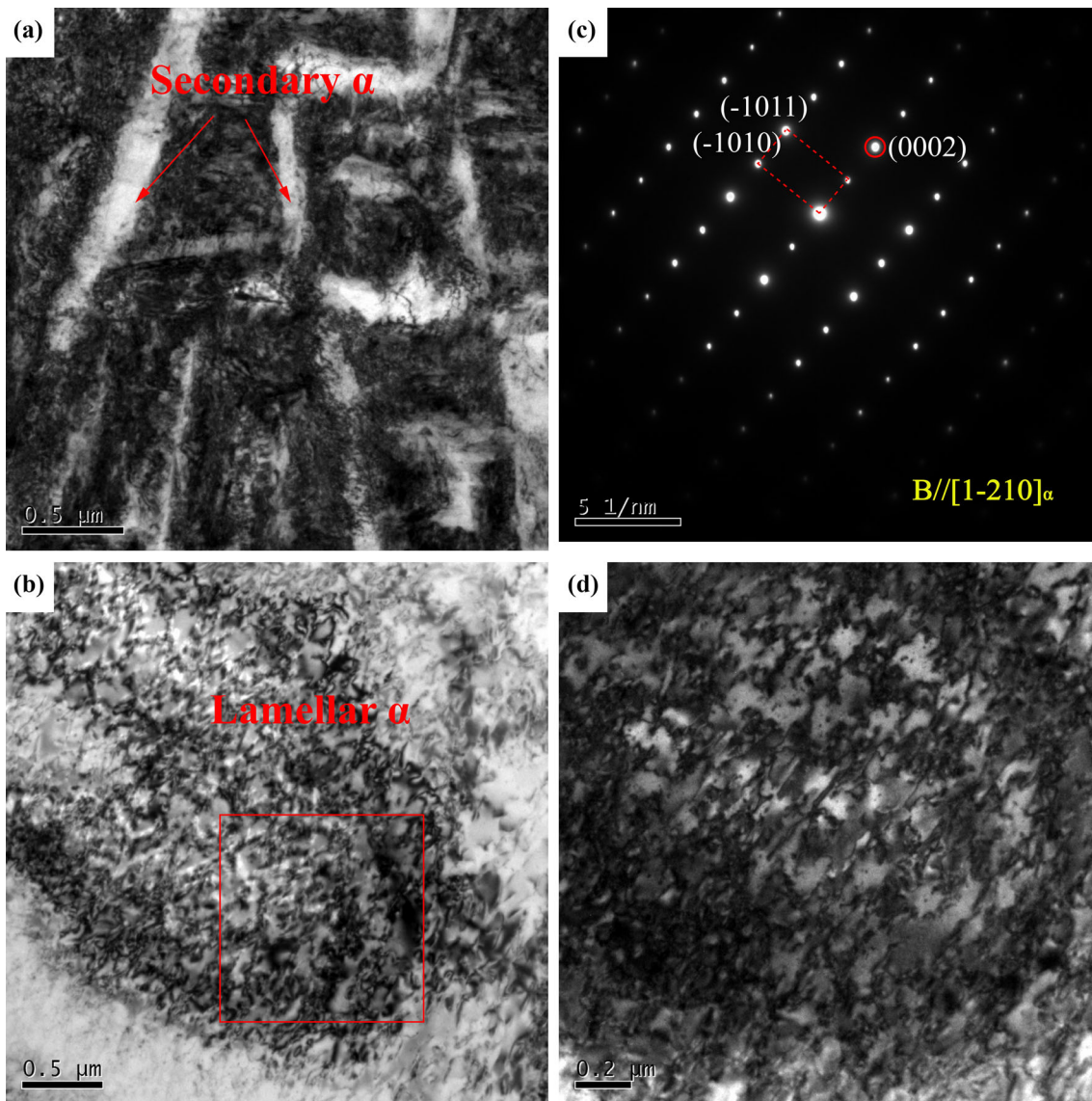


Fig. 11 Typical TEM morphologies of the lamellar α in the necked part of the ST920A450 tensile sample: (a) BF image of β -transformed structures displaying highly tangled dislocations piled up at the α_s/β interface; (b) BF image inside the lamellar α ; (c) diffraction spot of the lamellar α along the $[1210]\alpha$ zone axis; and (d) morphology of the dislocation cells through the $[0002]$ diffraction spots, circled by red circles in (c) (Color figure online)

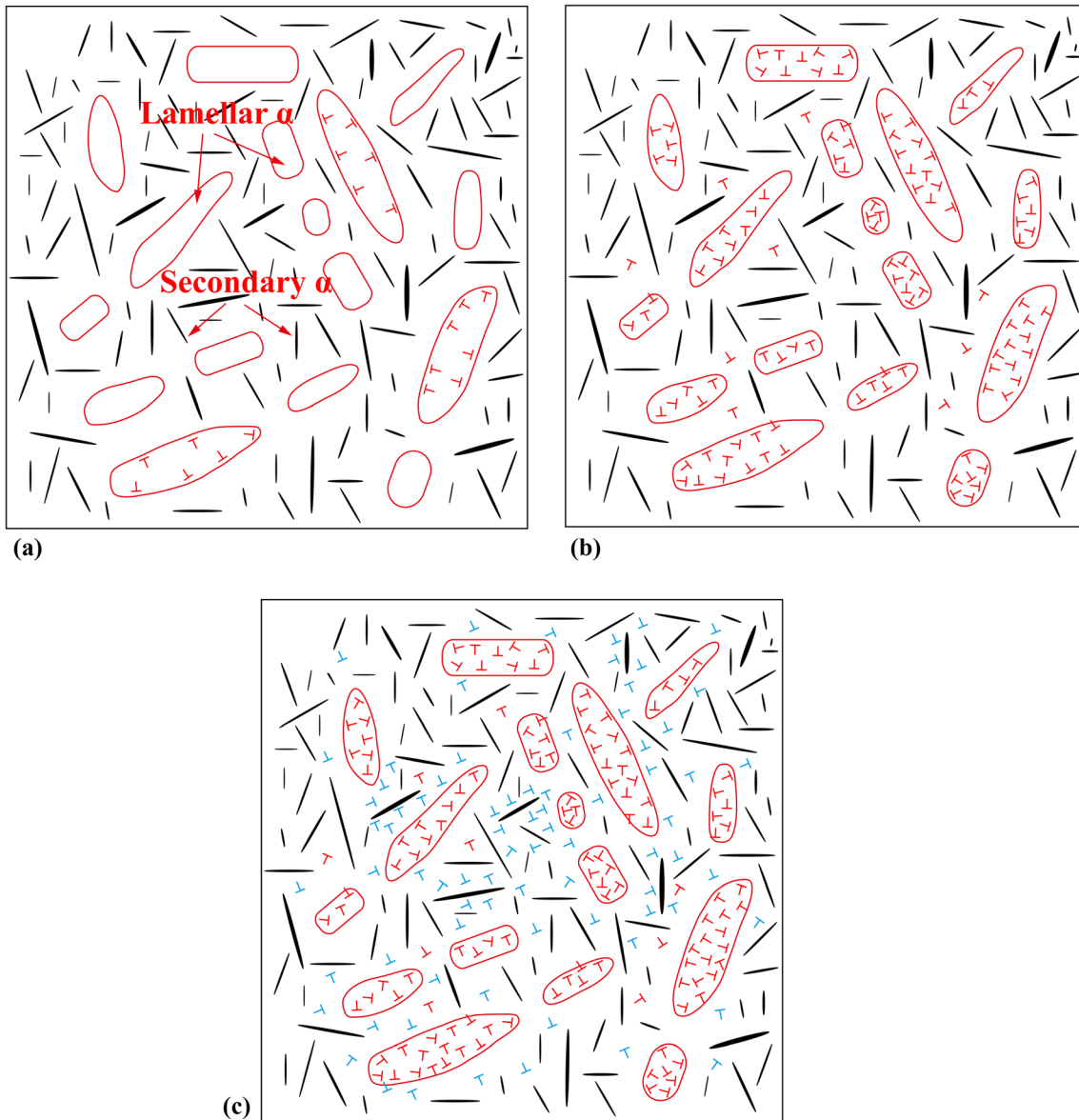


Fig. 12 Schematic of the microstructure evolution during tensile testing of the ST920A450 sample: (a) the initial tensile testing stage showing deformation feature inside lamellar α , (b) the following tensile testing stage showing deformation in the relatively soft lamellar α and work hardening resulting from dislocation accumulation and (c) the final tensile stage of the compatible deformation in the lamellar α and residual β phases

from continuous to discontinuous in the ST920A450 sample (Fig. 5a), and some dislocations could glide or penetrate easily across the grain boundary rather than piling up, which reduced the back stress and stress concentration along the grain boundary and simultaneously prohibited premature crack initiation and fracture (Ref 56, 57). Moreover, the propagation of cracks was more difficult through the discontinuous α_{GB} than for the continuous case.

A great deal of tangled dislocations provided good deformability for the lamellar α during the tensile process. Owing to the soft lamellar α , at the initial stage of strain, the initiation of plastic deformation commenced at the favorable lamellar α and then switched on the rest of the lamellar α . A

great number of dislocations in the tangled configuration and dislocation cells formed inside the lamellar α , which led to work hardening of the lamellar α , and hardened lamellar α boundaries were formed. With an increase in the applied stress, dislocations emerged in the transformed β structure and became piled up near the phase boundary, as shown in Fig. 12(a), which led to the plastic strain partitioning hierarchically. Afterward, at the onset of macroscopic deformation, both the lamellar α phases and transformed β structures deformed compatibly. Such deformation behavior and inhomogeneous strain partitioning are schematically illustrated in Fig. 12. Thus, the resultant inhomogeneous strain partition between the lamellar α and transformed β structures effectively improved

the ductility. Therefore, a promising combination of strength and ductility was accomplished through a high density of nanosized α_s , lamellar α and discontinuous α_{GB} .

5. Conclusions

In this paper, solid solution and aging treatments were performed on Ti-5.5Al-2Zr-1Mo-2.5V alloy pipe samples to tailor the microstructure and achieve good tensile strength and ductility. The conclusions are as follows.

- (1) The microstructure composed of lamellar α , discontinuous α_{GB} and β -transformed structures containing a high density of nanosized precipitates was obtained after solid solution and aging treatments.
- (2) The YS of the ST920A450 sample was improved significantly to 1064 MPa, and the EL remained at 10.5%. A promising combination of strength and ductility was achieved compared to those of the extruded alloy and requirements of ASTM B861. The highest UTS of 1328 MPa herein was obtained in the ST930S2.5A450 sample, yet the ductility dropped to 6.6%.
- (3) The high strength of the ST920A450 alloy was mainly derived from the resistance of the α_s/β interface to dislocation movement, while the excellent ductility was attributed to the effective strain partitioning and discontinuous α_{GB} .

Acknowledgments

This work was supported by the Project supported by State Key Laboratory of Powder Metallurgy of Central South University and by the National Science and Technology Major Project (2016ZX05020-002), Science and Technology Exploration Project of China National Petroleum Corporation (2018D-5010-08).

References

1. R.W. Schutz and H.B. Watkins, Recent Developments in Titanium Alloy Application in the Energy Industry, *Mater. Sci. Eng. A*, 1998, **243**, p 305–315
2. V.N. Moiseev, Structural Titanium Alloys in Modern Mechanical Engineering, *Met. Sci. Heat Treat.*, 2004, **46**, p 115–120
3. R.D. Kane, S. Craig, and A. Venkatesh, Titanium Alloys for Oil and Gas Service: A Review, in *CORROSION 2009, NACE International*, Atlanta, Georgia (2009), p. 21
4. C. Leyens and M. Peters, *Titanium and Titanium Alloys: Fundamentals and Applications*, Wiley, New York, 2003
5. R.Z. Li, C. Feng, L. Jiang, and Y.Q. Cao, Research Status and Development of Titanium Alloy Drill Pipes, *Mater. Sci. Forum.*, 2019, **944**, p 903–909
6. J.E. Smith, R.B. Chandler, and P.L. Boster, Titanium Drill Pipe for Ultra-Deep and Deep Directional Drilling, in *SPE/IADC Drilling Conference* (Society of Petroleum Engineers, Amsterdam, Netherlands, 2001), p. 14
7. J.E. Smith, R.W. Schutz, and E.I. Bailey, Development of Titanium Drill Pipe for Short Radius Drilling, in *IADC/SPE Drilling Conference* (Society of Petroleum Engineers, New Orleans, Louisiana, 2000), p. 11
8. M. Jellison and N. GrantPrideco, Lightweight, Ultra-High-Strength Drill Pipe May Meet Demands of ERD, Critical Deep Drilling, *Drill. Contract.*, 2009, **3**, p 53–56
9. R. Gaur, R.K. Gupta, V. AnilKumar, and S.S. Banwait, Effect of Cold Rolling and Heat Treatment on Microstructure and Mechanical Properties of Ti-4Al-1Mn Titanium Alloy, *J. Mater. Eng. Perform.*, 2018, **27**, p 3217–3233
10. Y. Yu, S. Hui, W. Ye, and B. Xiong, Mechanical Properties and Microstructure of an $\alpha + \beta$ Titanium Alloy with High Strength and Fracture Toughness, *Rare Met.*, 2009, **28**, p 346–349
11. P.F. Gao, G. Qin, X.X. Wang, Y.X. Li, M. Zhan, G.J. Li, and J.S. Li, Dependence of Mechanical Properties on the Microstructural Parameters of TA15 Titanium Alloy with Tri-Modal Microstructure, *Mater. Sci. Eng. A*, 2019, **739**, p 203–213
12. P. Guo, Y. Zhao, W. Zeng, and J. Liu, Effect of Microstructure on the Fatigue Crack Propagation Behavior of TC4-DT Titanium Alloy, *J. Mater. Eng. Perform.*, 2015, **24**, p 1865–1870
13. Z.N. Lei, P.F. Gao, H.W. Li, Y. Cai, Y.X. Li, and M. Zhan, Comparative Analyses of the Tensile and Damage Tolerance Properties of Tri-Modal Microstructure to Widmanstätten and Bimodal Microstructures of TA15 Titanium Alloy, *J. Alloys Compd.*, 2019, **788**, p 831–841
14. C. Li, J. Chen, W. Li, J.J. He, W. Qiu, Y.J. Ren, J.L. Chen, and J.H. Chen, Study on the Relationship Between Microstructure and Mechanical Property in a Metastable β Titanium Alloy, *J. Alloys Compd.*, 2015, **627**, p 222–230
15. A. Gheysarian and M. Abbasi, The Effect of Aging on Microstructure, Formability and Springback of Ti-6Al-4V Titanium Alloy, *J. Mater. Eng. Perform.*, 2017, **26**, p 374–382
16. A.P. Mouritz, Titanium Alloys for Aerospace Structures and Engines, *Introduction to Aerospace Materials*, Woodhead Publishing, 2012, p 202–223
17. G. Lütjering and J.C. Williams, *Titanium*, Springer, Berlin, 2007, p 227–229
18. Y. Chong, G. Deng, S. Gao, J. Yi, A. Shibata, and N. Tsuji, Yielding Nature and Hall-Petch Relationships in Ti-6Al-4V Alloy with Fully Equiaxed and Bimodal Microstructures, *Scr. Mater.*, 2019, **172**, p 77–82
19. H. Wu, Z. Sun, J. Cao, and Z. Yin, Microstructure and Mechanical Behavior of Heat-Treated and Thermomechanically Processed TA15 Ti Alloy Composites, *J. Mater. Eng. Perform.*, 2019, **28**, p 788–799
20. I. Weiss and S.L. Semiatin, Thermomechanical Processing of Alpha Titanium Alloys: An Overview, *Mater. Sci. Eng. A*, 1999, **263**, p 243–256
21. G. Lütjering, Influence of Processing on Microstructure and Mechanical Properties of ($\alpha + \beta$) Titanium Alloys, *Mater. Sci. Eng. A.*, 1998, **243**, p 32–45
22. J. Fan, J.S. Li, H. Kou, K. Hua, and B. Tang, The Interrelationship of Fracture Toughness and Microstructure in a New Near β Titanium Alloy Ti-7Mo-3Nb-3Cr-3Al, *Mater. Charact.*, 2014, **96**, p 93–99
23. J.D. Paramore, Z.Z. Fang, P. Sun, M. Koopman, K.S.R. Chandran, and M. Dunstan, A Powder Metallurgy Method for Manufacturing Ti-6Al-4V with Wrought-Like Microstructures and Mechanical Properties Via Hydrogen Sintering and Phase Transformation (HSPT), *Scr. Mater.*, 2015, **107**, p 103–106
24. H.Z. Niu, H.R. Zhang, Q.Q. Sun, and D. Zhang, Breaking Through the Strength-Ductility Trade-Off Dilemma in Powder Metallurgy Ti 6Al 4V Titanium Alloy, *Mater. Sci. Eng. A*, 2019, **754**, p 361–369
25. Y. Chen, Z. Du, S. Xiao, L. Xu, and J. Tian, Effect of Aging Heat Treatment on Microstructure and Tensile Properties of a New β High Strength Titanium Alloy, *J. Alloys Compd.*, 2014, **586**, p 588–592
26. S.A. Mantri, D. Choudhuri, A. Behera, J.D. Cotton, N. Kumar, and R. Banerjee, Influence of Fine-Scale Alpha Precipitation on the Mechanical Properties of the Beta Titanium Alloy Beta-21S, *Metall. Mater. Trans. A.*, 2015, **46**, p 2803–2808
27. K. Yue, L. Jianrong, Z. Shaoxiang, W. Lei, W. Qingjiang, and Y. Rui, Origins of Different Tensile Behaviors Induced by Cooling Rate in a Near Alpha Titanium Alloy Ti65, *Materialia*, 2018, **1**, p S603383428
28. S.A. Mantri, D. Choudhuri, T. Alam, G.B. Viswanathan, J.M. Sosa, H.L. Fraser, and R. Banerjee, Tuning the Scale of α Precipitates in β -Titanium Alloys for Achieving High Strength, *Scr. Mater.*, 2018, **154**, p 139–144
29. M.T. Jia, D.L. Zhang, B. Gabbitas, J.M. Liang, and C. Kong, A Novel Ti-6Al-4V Alloy Microstructure with Very High Strength and Good Ductility, *Scr. Mater.*, 2015, **107**, p 10–13

30. F. Geng, M. Niinomi, and M. Nakai, Observation of Yielding and Strain Hardening in a Titanium Alloy Having High Oxygen Content, *Mater. Sci. Eng. A*, 2011, **528**, p 5435–5445
31. W.Y. Guo, H. Xing, J. Sun, X.L. Li, J.S. Wu, and R. Chen, Evolution of Microstructure and Texture during Recrystallization of the Cold-Swaged Ti-Nb-Ta-Zr-O Alloy, *Met. Mater. Trans. A.*, 2008, **39**, p 672–678
32. Y. Okazaki, Y. Ito, A. Ito, and T. Tateishi, Effect of Alloying Elements on Mechanical Properties of Titanium Alloys for Medical Implants, *Mater. Trans. JIM*, 1993, **34**, p 1217–1222
33. G.C. Obasi, S. Biroscas, D.G. Leo Prakash, J.Q. Da Fonseca, and M. Preuss, The Influence of Rolling Temperature on Texture Evolution and Variant Selection During $\alpha \rightarrow \beta \rightarrow \alpha$ Phase Transformation in Ti-6Al-4V, *Acta Mater.*, 2012, **60**, p 6013–6024
34. Z. Sun, H. Wu, J. Sun, and C. Jing, Evolution of Lamellar α Phase During Two-Phase Field Heat Treatment in TA15 Alloy, *Int. J. Hydrog. Energy*, 2017, **42**, p 20849–20856
35. H. Wu, Z. Sun, J. Cao, and Z. Yin, Formation and Evolution of Tri-Modal Microstructure During Dual Heat Treatment for TA15 Ti-Alloy, *J. Alloys Compd.*, 2019, **786**, p 894–905
36. Z. Zhao, J. Chen, H. Tan, G. Zhang, X. Lin, and W. Huang, Achieving Superior Ductility for Laser Solid Formed Extra Low Interstitial Ti-6Al-4V Titanium Alloy Through Equiaxial Alpha Microstructure, *Scr. Mater.*, 2018, **146**, p 187–191
37. X. Gao, W. Zeng, Y. Wang, Y. Long, S. Zhang, and Q. Wang, Evolution of Equiaxed Alpha Phase During Heat Treatment in a Near Alpha Titanium Alloy, *J. Alloys Compd.*, 2017, **725**, p 536–543
38. Z. Du, S. Xiao, L. Xu, J. Tian, F. Kong, and Y. Chen, Effect of Heat Treatment on Microstructure and Mechanical Properties of a New β High Strength Titanium Alloy, *Mater. Des.*, 2014, **55**, p 183–190
39. Y. Zhang, J.P. Liu, S.Y. Chen, X. Xie, P.K. Liaw, K.A. Dahmen, J.W. Qiao, and Y.L. Wang, Serration and Noise Behaviors in Materials, *Prog. Mater. Sci.*, 2017, **90**, p 358–460
40. W.C.P. ASTM International. ASTM B861 - 14 Standard Specification for Titanium and Titanium Alloy Seamless Pipe (2014), pp. B814–B861
41. Q.Y. Sun and H.C. Gu, Tensile and Low-Cycle Fatigue Behavior of Commercially Pure Titanium and Ti-5Al-2.5Sn Alloy at 293 and 77 K, *Mater. Sci. Eng. A.*, 2001, **316**, p 80–86
42. H.F. Lu, K.Y. Luo, L.J. Wu, C.Y. Cui, and J.Z. Lu, Effects of Service Temperature on Tensile Properties and Microstructural Evolution of CP Titanium Subjected to Laser Shock Peening, *J. Alloys Compd.*, 2019, **770**, p 732–741
43. S. Zhrebtsov, E. Kudryavtsev, S. Kostjuchenko, S. Malysheva, and G. Salishchev, Strength and Ductility-Related Properties of Ultrafine Grained Two-Phase Titanium Alloy Produced by Warm Multiaxial Forging, *Mater. Sci. Eng. A*, 2012, **536**, p 190–196
44. W. Lee, T. Chen, and H. Hwang, Impact Response and Microstructural Evolution of Biomedical Titanium Alloy Under Various Temperatures, *Metall. Mater. Trans. A.*, 2008, **2008**(39), p 1435–1448
45. M. Wan, Y. Zhao, W. Zeng, and G. Cai, Effects of Cold Pre-Deformation on Aging Behavior and Mechanical Properties of Ti-1300 Alloy, *J. Alloys Compd.*, 2015, **619**, p 383–388
46. Z. Lincai, D. Xiaoming, Y. Wei, Z. Man, and S. Zhenya, Effect of Prestrain on Precipitation Behaviors of Ti-2.5Cu Alloy, *High Temp. Mater. Process.*, 2017, **37**, p 487–493
47. W. Zhu, J. Lei, Z. Zhang, Q. Sun, W. Chen, L. Xiao, and J. Sun, Microstructural Dependence of Strength and Ductility in a Novel High Strength β Titanium Alloy with Bi-Modal Structure, *Mater. Sci. Eng. A*, 2019, **762**, p 138086
48. A.H. Rosenberger, A. Madsen, and H. Ghonem, Aging Effects on the Creep Behavior of the Near-Alpha Titanium Alloy Ti-1100, *J. Mater. Eng. Perform.*, 1995, **4**, p 182–187
49. E.O. Hall, The Deformation and Ageing of Mild Steel: III, Discussion of Results, *Proc. Phys. Soc. Sect. B.*, 1951, **64**, p 747–753
50. X. Wen, M. Wan, C. Huang, Y. Tan, M. Lei, Y. Liang, and X. Cai, Effect of Microstructure on Tensile Properties, Impact Toughness and Fracture Toughness of TC21 Alloy, *Mater. Des.*, 2019, **180**, p 107898
51. Z.X. Zhang, S.J. Qu, A.H. Feng, and J. Shen, Achieving Grain Refinement and Enhanced Mechanical Properties in Ti-6Al-4V Alloy Produced by Multidirectional Isothermal Forging, *Mater. Sci. Eng. A*, 2017, **692**, p 127–138
52. J. Málek, F. Hnilica, J. Veselý, B. Smola, and R. Medlín, The Effect of Annealing Temperature on the Properties of Powder Metallurgy Processed Ti-35Nb-2Zr-0.5O Alloy, *J. Mech. Behav. Biomed.*, 2017, **75**, p 252–261
53. P. Luo, D.T. McDonald, W. Xu, S. Palanisamy, M.S. Dargusch, and K. Xia, A Modified Hall-Petch Relationship in Ultrafine-Grained Titanium Recycled from Chips by Equal Channel Angular Pressing, *Scr. Mater.*, 2012, **66**, p 785–788
54. Z. Wang, Cyclic Deformation Response of Planar-Slip Materials and a New Criterion for the Wavy-to-Planar-Slip Transition, *Philos. Mag.*, 2004, **84**, p 351–379
55. D. Caillard, M. Gaumé, and F. Onimus, Glide and Cross-Slip of a-Dislocations in Zr and Ti, *Acta Mater.*, 2018, **155**, p 23–34
56. C.S.G. Lütjering, Influence of α Layers at β Grain Boundaries on Mechanical Properties of Ti-Alloys, *Mater. Sci. Eng. A*, 2001, **319**, p 393–397
57. J.W. Foltz, B. Welk, P.C. Collins, H.L. Fraser, and J.C. Williams, Formation of Grain Boundary α in β Ti Alloys: Its Role in Deformation and Fracture Behavior of These Alloys, *Metall. Mater. Trans. A*, 2011, **42**, p 645–650

Publisher's Note Springer Nature remains neutral with regard to jurisdictional claims in published maps and institutional affiliations.